PHYSICAL REVIEW C **74**, 054314 (2006)

Multiple band structures in ^{169}Ta

D. J. Hartley, W. H. Mohr, and J. R. Vanhoy
Department of Physics, U.S. Naval Academy, Annapolis, Maryland 21402, USA

M. A. Riley, A. Aguilar, and C. Teal
Department of Physics, Florida State University, Tallahassee, Florida 32306, USA

R. V. F. Janssens, M. P. Carpenter, A. A. Hecht, T. Lauritsen, E. F. Moore, and S. Zhu
Physics Division, Argonne National Laboratory, Argonne, Illinois 60439, USA

F. G. Kondev
Nuclear Engineering Division, Argonne National Laboratory, Argonne, Illinois 60439, USA

M. K. Djongolov, M. Danchev, and L. L. Riedinger
Department of Physics and Astronomy, University of Tennessee, Knoxville, Tennessee 37996, USA

G. B. Hagemann and G. Sletten
Niels Bohr Institute, Blegdamsvej 17, DK-2100 Copenhagen, Denmark

P. Chowdhury and S. K. Tandel
Department of Physics, University of Massachusetts Lowell, Lowell, Massachusetts 01854, USA

W. C. Ma
Department of Physics, Mississippi State University, Mississippi State, Mississippi 39762, USA

S. W. Ødegård
Department of Physics, University of Oslo, PB 1048 Blindern, N-0316 Oslo, Norway
(Received 5 September 2006; published 28 November 2006)

Rotational structures in the ^{169}Ta nucleus were studied via the ^{124}Sn(^{51}V, $6n$) reaction. These data were obtained as a side channel of an experiment focusing on ^{171}Ta, but the sensitivity provided by the Gammasphere spectrometer proved sufficient for a significant extension of the level scheme of this rare-earth nucleus. Over 170 new transitions and four new band structures were placed in ^{169}Ta, including the intruder $\pi i_{13/2}$ structure. Linking transitions between all of the sequences were identified, and the relative excitation energies between the different configurations were determined for the first time. The rotational sequences were interpreted within the framework of the cranked shell model.

DOI: 10.1103/PhysRevC.74.054314 PACS number(s): 21.10.Re, 23.20.Lv, 27.70.+q

I. INTRODUCTION

The intruder proton orbitals of the mass-170 region have recently drawn attention because of their anomalous behavior. Collective structures based on the $i_{13/2}$ proton orbital have been the focus of many studies of Lu nuclei, as wobbling excitations have been observed in ^{161,163,165,167}Lu [1–6]. This collective mode indicates that stable triaxial deformation is present in these nuclei over a wide range of spin and energy. However, no examples of wobbling have been identified thus far outside the Lu nuclei, raising the following questions: Are these Lu nuclei unique? Or will triaxial deformation be observed in a broader region of nuclei? These issues provided the motivation for the present experiment which undertook a search for wobbling sequences based on the $i_{13/2}$ bands in Ta nuclei. An $i_{13/2}$ structure was previously known only in ^{171}Ta [7,8]; therefore, it was the primary nucleus of interest for this study. Results from the ^{171}Ta data have been published [9]. However, significant data on ^{169}Ta were also collected during the experiment. This paper reports on new results obtained for ^{169}Ta, including the identification of the $\pi i_{13/2}$ structure.

In addition to the shape-driving properties of the $i_{13/2}$ orbital, the $\pi h_{9/2}$ bands have also displayed unusual characteristics in the odd-proton, $A \approx 170$ nuclei. Significantly delayed crossings are observed in these bands with respect to the even-even neighbors [10]. Initially, the increased deformation associated with this configuration was suggested as the cause of the delay [11]. However, more recent interpretations invoke proton-neutron interactions, along with the larger deformation, to account for the delayed crossings [12]. This phenomenon is investigated in this work with the cranked shell model, using empirically derived pairing energies. A previous publication on ^{169}Ta [13] also identified a second crossing in the

$h_{9/2}$ band. However, the present data indicate that some transitions were improperly associated with this sequence. Therefore, this second backbend is no longer present.

Three additional new structures were observed in ^{169}Ta; they have been assigned configurations based on their inband properties. Furthermore, all previously known bands were extended to higher spins, and a second crossing has now been identified in some of them near a rotational frequency of 0.4 MeV. Finally, all of the sequences have been linked together for the first time, so their relative excitation energies have been determined. A systematic comparison of the experimental bandhead energies is made with the predictions of Nazarewicz, Riley, and Garrett [14] for the Ta nuclei.

II. EXPERIMENTAL DETAILS

In an experiment optimized to produce high-spin states in ^{171}Ta [9], a significant amount of new data was collected for the ^{169}Ta nucleus. The ^{124}Sn(^{51}V, $6n$) reaction populated these states, where the ^{51}V beam was accelerated to 228 MeV by the Argonne Tandem-Linac Accelerator System (ATLAS) facility at Argonne National Laboratory. Two self-supporting foils of ^{124}Sn were used, each having a thickness of $\sim$500 μg/cm^2. Approximately 2×10^9 events were detected in the Gammasphere [15] array following a software gate on the prompt ($\sim$80 ns) γ rays. Gammasphere consisted of 100 Compton-suppressed detectors for this experiment. The data were then sorted into a Blue database [16] to facilitate quick creation of various coincidence histograms and spectra, which included RadWare [17] cubes and hypercubes to determine the γ-ray coincidence relationships. In addition, angle-dependent spectra were generated from the Blue database to perform an angular correlation ratio analysis such that spins could be assigned to newly observed states. Details of this angular correlation ratio analysis may be found in Ref. [9], along with other relevant experimental details.

III. LEVEL SCHEME

Low-spin states in ^{169}Ta were first confirmed by Meissner *et al.* [18] through the investigation of the electron-capture/β^+ decay of ^{169}W. This study produced a tentative $5/2^+$ assignment for the ground state of ^{169}Ta. Meissner *et al.* interpreted this level as the bandhead state associated with the [402]5/2 configuration of $d_{5/2}$ parentage. A high-spin experiment for ^{169}Ta was published later by Li *et al.* [13], where five rotational bands were reported. Sequences based on the $d_{5/2}$[402]5/2, $h_{11/2}$[514]9/2, $h_{9/2}$[541]1/2, and $d_{3/2}$[411]1/2 protons were identified in that work. However, none of the structures were linked together; therefore, the relative excitations energies were not previously known. The [411]1/2 band was extended to higher spins by Song *et al.* [19], while lifetimes on the order of nanoseconds were measured for the [541]1/2 and [514]9/2 bandhead states by Zhang *et al.* [20,21].

Four new bands were observed in the present experiment, and approximately 300 transitions (170 more than previously known) are now confirmed in ^{169}Ta. The resulting level scheme is presented in Fig. 1. The parity of the states has never been directly measured; therefore, all parity assignments are based on the proposed configuration of the bands. Note that all of the bands have been linked together. Hence, the energies associated with various excitations are now known. Due to the complexity of the level scheme and the numerous transitions at low spin, a partial level scheme is provided in Fig. 2 that clearly displays the low-spin, low-excitation-energy region. Table I summarizes the level energies and γ-ray energies, intensities, and angular correction ratios determined for ^{169}Ta.

A. Band 1

The bandhead level of band 1 was determined to be the ground state of ^{169}Ta based on the various linking transitions observed in Figs. 1 and 2. This strongly coupled sequence was previously associated with the [402]5/2 configuration [13], and we are in agreement with this assignment (see Sec. IV A). Thus, this interpretation is consistent with the proposed $5/2^+$ ground-state assignment of Meissner *et al.* [18]. The observed coincidence γ-ray relationships suggest a different interpretation for the $7/2^+$ states located at 96 and 136 keV (see Fig. 2) with respect to those found in Refs. [13,18]. The 96-keV level was previously assigned as the bandhead for the [404]7/2 sequence, while the 136-keV state was suggested to be the first excited state in the [402]5/2 sequence. Such an interpretation would require a 285-keV cross-over transition from the $9/2^+$ level to the $5/2^+$ state in band 1 as seen in Ref. [13]. However, no evidence was found for the 285-keV transition, as can be verified in the sample spectrum of band 1 displayed in Fig. 3(a). Instead, a 245-keV line decaying from the $9/2^+$ state appears to be the cross-over transition, and this finding strongly suggests that the 96-keV level is a member of the [402]5/2 sequence. The 136-keV state is now interpreted as being the bandhead for the [404]7/2 structure (see below). Note that several new linking transitions between bands 1 and 2 were observed as shown in Fig. 1. The presence of these many linking transitions indicates that the two structures likely share the same parity and have a large overlap in their wave functions. Band 1 was extended from spin 57/2 to 69/2, and it is the energetically lowest positive-parity sequence throughout the entire spin range. This is seen in Fig. 4(a) which plots the energy of the states minus a rigid-rotor reference versus spin. However, the negative-parity bands 5 and 8, shown in Fig. 4(b), compose the yrast line above $I = 9/2$.

B. Band 2

The strongly coupled sequence labeled as band 2 in Fig. 1 is a new structure that, as mentioned above, is linked through a series of transitions to band 1. Several of these linking transitions have angular correlation ratios near 0.8 (see Table I) which is between the pure dipole and quadrupole values of 0.6 and 1.0, respectively. Therefore, these γ rays likely correspond to $M1/E2$, $\Delta I = 1$ transitions, and this results in the proposed spin/parity assignments for band 2 indicated in Fig. 1. The spectrum in Fig. 3(b) displays the lower portion of the band, while the inset presents the extension of the

FIG. 1. Proposed level scheme for ^{169}Ta; arrow width is proportional to the relative intensity of the γ rays. Tentative transitions and levels are denoted with dashed lines.

TABLE I. γ-ray energies and intensities in ^{169}Ta.

I^{π} [a]	E_{level} (keV)	E_{γ} (keV) [b]	I_{γ} [c]	Ang. Corr. Ratio
	Band 1: [402]5/2 $\alpha = +1/2$			
$\frac{5}{2}^+$	0.0			
$\frac{9}{2}^+$	244.7	244.7	11.3(8) [d]	
		148.3	59(2) [d]	0.68(4)
		109.0	10.3(5) [d]	0.53(9)
$\frac{13}{2}^+$	616.9	372.2	59(2)	0.85(4)
		196.8	37(1)	0.69(4)
		129.2	4.1(3)	
$\frac{17}{2}^+$	1069.7	452.8	52(2)	0.98(4) [e]
		233.8	15.3(7)	0.83(5)
$\frac{21}{2}^+$	1581.2	511.5	45(2)	0.96(4)
		259.8	12.7(6)	0.73(5)
$\frac{25}{2}^+$	2129.9	548.7	43(2)	1.08(5) [e]
		274.7	11.6(4)	0.54(4) [e]
$\frac{29}{2}^+$	2634.8	504.9	35(2)	0.97(5)
		229.3	15.9(7)	0.68(6)
		429.0	3.5(5)	
$\frac{33}{2}^+$	3053.6	418.8	17(1)	1.0(1)
		208.8	15(2)	0.69(3) [e]
$\frac{37}{2}^+$	3541.0	487.4	14(1)	1.15(8)
		244.3	8.3(8)	0.69(3) [e]
$\frac{41}{2}^+$	4110.0	569.0	15(1)	0.87(8)
		280.4	5.3(8)	0.63(5)
$\frac{45}{2}^+$	4750.6	640.6	11.8(9)	1.14(8)
		311.8	4.5(8)	
$(\frac{49}{2}^+)$	5450.0	699.4	10.3(7)	
		338.6	2.7(6)	
$(\frac{53}{2}^+)$	6195.1	745.1	5.6(8)	
		360.3	1.8(3)	
$(\frac{57}{2}^+)$	6978.4	783.3	4.2(7)	
$(\frac{61}{2}^+)$	7810.0	831.6	2.7(6)	
$(\frac{65}{2}^+)$	8695.0	885.0	1.6(3)	
$(\frac{69}{2}^+)$	9635	940	<1	
	Band 1: [402]5/2 $\alpha = -1/2$			
$\frac{7}{2}^+$	96.4	96.4	~45 [f]	0.55(9)
$\frac{11}{2}^+$	420.1	323.7	27(2)	0.81(5)
		175.3	62(1)	0.73(4)
		122.1	4.8(5)	
$\frac{15}{2}^+$	836.0	415.9	54(2)	0.96(5)
		218.9	25(1)	0.74(4)
		140.0	1.7(4)	
$\frac{19}{2}^+$	1321.2	485.2	47(2)	1.15(4) [e]
		251.5	13.2(7)	0.78(5)
$\frac{23}{2}^+$	1855.0	533.8	44(4)	1.06(5) [e]
		274.0	13.6(8)	0.54(4) [e]
$\frac{27}{2}^+$	2405.4	550.4	41(2)	1.08(5) [e]
		275.5	10.3(9)	0.54(4) [e]
$\frac{31}{2}^+$	2845.0	439.6	20(1)	1.11(6) [e]
		210.2	17.1(8)	0.69(3) [e]
$\frac{35}{2}^+$	3296.9	451.9	13.5(6)	0.98(4) [e]
		243.1	13.1(6)	0.69(3) [e]
$\frac{39}{2}^+$	3829.8	532.9	12.7(5)	1.06(5) [e]
		288.6	6.7(7)	0.67(6)
$\frac{43}{2}^+$	4438.7	608.9	12.7(5)	0.92(6)
		328.8	5.3(6)	0.61(6)
$(\frac{47}{2}^+)$	5111.2	672.5	10.7(5)	1.10(8)
		360.6	3.1(5)	0.76(5)
$(\frac{51}{2}^+)$	5834.6	723.4	7.1(6)	1.04(9)
		384.8	2.2(3)	0.59(5)
$(\frac{55}{2}^+)$	6599.2	764.6	3.6(5)	
		(404)	<1	
$(\frac{59}{2}^+)$	7409.2	810.0	1.1(2)	
$(\frac{63}{2}^+)$	(8279)	(870)	<1	
	Band 2: [404]7/2 $\alpha = +1/2$			
$\frac{9}{2}^+$	298.0	162.3	~30 [d]	0.64(4)
		201.5	~6.6 [d]	0.71(6)
		298.0	~11 [d]	1.00(6)
$\frac{13}{2}^+$	695.9	397.9	26(2)	0.91(5)
		208.4	14.0(7)	0.77(5)
		275.8	3.6(4)	0.84(6)
$\frac{17}{2}^+$	1170.5	474.6	29(3)	0.70(5)
		242.5	10.2(6)	0.85(5) [e]
		334.7	3.9(4)	
$\frac{21}{2}^+$	1697.5	527.0	30(2)	1.01(4)
		264.6	6.2(7)	0.69(7) [e]
		376.4	3.6(4)	
$\frac{25}{2}^+$	2257.5	560.0	13.9(9)	1.00(5)
		280.2	6.2(6)	0.79(5) [e]
$\frac{29}{2}^+$	2711.7	(454)	<1	
		581.8	10.0(8)	1.2(1)
		305.9	1.6(2)	
		377.0	<1	
$\frac{33}{2}^+$	3150.3	438.6	7.1(6)	1.03(6) [e]
$(\frac{37}{2}^+)$	3653.0	502.7	6.4(7)	
$(\frac{41}{2}^+)$	4240.5	587.5	4.1(4)	
$(\frac{45}{2}^+)$	4903.3	662.8	3.6(3)	
$(\frac{49}{2}^+)$	5627.6	724.3	2.9(3)	
$(\frac{53}{2}^+)$	6391.4	763.8	2.1(2)	
$(\frac{57}{2}^+)$	7195.1	803.7	<1	
	Band 2: [404]7/2 $\alpha = -1/2$			
$\frac{7}{2}^+$	135.7	135.7	~45 [f]	0.64(3)
$\frac{11}{2}^+$	487.7	352.0	16.8(9) [d]	0.92(5)
		189.6	23(1) [d]	0.70(4)
		242.9	5.7(6) [d]	0.85(5) [e]
$\frac{15}{2}^+$	927.9	440.2	29(2)	1.03(6) [e]
		232.0	12.6(9)	0.72(5)
		311.0	7.3(6)	0.80(9)
$\frac{19}{2}^+$	1432.8	504.9	24(2)	1.02(5)
		262.2	7.5(6)	0.69(7) [e]
		363.3	4.1(5)	
$\frac{23}{2}^+$	1976.9	544.1	18(1)	0.89(6)
		279.5	4.9(5)	0.79(5) [e]
$\frac{27}{2}^+$	2498.7	521.8	14.2(9)	1.2(1)
		241.6	4.9(5)	0.85(5) [e]

TABLE I. *(Continued.)*

I^{π} [a]	E_{level} (keV)	E_{γ} (keV)[b]	I_{γ} [c]	Ang. Corr. Ratio
$\frac{31}{2}^+$	2940.4	441.7	7.9(6)	1.03(6)[e]
		(535)	<1	
$\frac{35}{2}^+$	3402.1	461.7	4.4(3)	0.97(5)
$\frac{39}{2}^+$	3951.9	549.8	3.8(3)	0.98(5)
$(\frac{43}{2}^+)$	4581.9	630.0	3.1(3)	
$(\frac{47}{2}^+)$	5278.8	696.9	2.1(2)	
$(\frac{51}{2}^+)$	6024.1	745.3	1.0(2)	
$(\frac{55}{2}^+)$	6812.3	788.2	<1	
	Band 3: [660]1/2			
$\frac{21}{2}^+$	1875.1	381.4	1.7(2)	
		570.4	4.3(3)	0.94(9)
$\frac{25}{2}^+$	2205.6	330.5	2.8(3)	
		416.5	15.1(9)	0.95(4)
		508.4	10.8(8)	1.0(1)[e]
		(624)	<1	
$\frac{29}{2}^+$	2667.3	461.7	25(2)	0.98(5)
		262.2	3.6(3)	
		410.1	3.3(3)	
$\frac{33}{2}^+$	3176.6	509.3	14(2)	1.05(9)
		(431)	<1	
		(542)	<1	
$\frac{37}{2}^+$	3741.8	565.2	10.2(7)	0.8(1)
		568.3	5.6(6)	1.2(2)
$\frac{41}{2}^+$	4360.9	619.1	10.5(7)	0.82(8)
$\frac{45}{2}^+$	5031.0	670.1	7.4(6)	0.8(1)
$(\frac{49}{2}^+)$	5746.7	715.7	6.1(5)	
$(\frac{53}{2}^+)$	6521.4	774.7	2.2(2)	
$(\frac{57}{2}^+)$	7327.7	806.3	<1	
$(\frac{61}{2}^+)$	8182.3	854.6	<1	
$(\frac{65}{2}^+)$	9085.3	903.0	<1	
	Band 4: [411]1/2 $\alpha = +1/2$			
$\frac{1}{2}^+$	11.2			
$\frac{5}{2}^+$	179.7	168.5	~5[d]	0.9(2)
		152.4	~26[d]	0.71(5)
$\frac{9}{2}^+$	466.0	286.3	26(2)	0.80(4)
		232.6	25(2)	0.61(4)
$\frac{13}{2}^+$	848.7	382.7	33(3)	0.90(5)
		280.4	10.2(8)	0.65(6)
$\frac{17}{2}^+$	1304.1	455.4	26(2)	0.90(4)
		304.8	2.6(2)	
$\frac{21}{2}^+$	1789.1	485.0	21(2)	0.99(5)
		295.7	2.1(2)	
$\frac{25}{2}^+$	2335.1	546.0	5.0(4)	1.0(1)
		459.9	3.3(3)	
$(\frac{29}{2}^+)$	2745.6	410.5	2.6(2)	
		(488)	<1	
$(\frac{33}{2}^+)$	3173.1	(428)	<1	0.97(9)
		505.8	10.1(9)	
$(\frac{37}{2}^+)$	3689.0	515.9	5.6(6)	
		512.6	3.1(4)	

TABLE I. *(Continued.)*

I^{π} [a]	E_{level} (keV)	E_{γ} (keV)[b]	I_{γ} [c]	Ang. Corr. Ratio
$(\frac{41}{2}^+)$	4285.3	596.3	6.0(5)	
$(\frac{45}{2}^+)$	4947.9	662.6	3.1(3)	
$(\frac{49}{2}^+)$	5642.0	694.1	1.4(2)	
$(\frac{53}{2}^+)$	6351.0	709.0	<1	
	Band 4: [411]1/2 $\alpha = -1/2$			
$\frac{3}{2}^+$	27.3			
$\frac{7}{2}^+$	233.1	205.8	49[d]	0.80(5)
		(53)		
$\frac{11}{2}^+$	568.2	335.1	44(3)	0.83(4)
$\frac{15}{2}^+$	999.2	431.0	37(3)	0.89(4)
$\frac{19}{2}^+$	1493.5	494.3	34(3)	0.86(6)
		635.0	<1	
$\frac{23}{2}^+$	2017.4	523.9	29(3)	0.94(5)
		720.8	2.9(2)	
$\frac{27}{2}^+$	2530.7	513.3	22(2)	0.86(5)
		710.2	3.6(3)	
$\frac{31}{2}^+$	2986.7	456.0	15.6(8)	1.11(9)
		574.3	<1	
$\frac{35}{2}^+$	3462.0	475.3	13.5(7)	1.19(8)
$\frac{39}{2}^+$	4020.0	558.0	9.8(6)	1.4(1)
$\frac{43}{2}^+$	4651.6	631.6	5.6(5)	
$(\frac{47}{2}^+)$	5354.9	703.3	2.1(2)	
$(\frac{51}{2}^+)$	6104.2	749.3	1.1(2)	
$(\frac{55}{2}^+)$	6887.9	783.7	<1	
	Band 5: [541]1/2 $\alpha = +1/2$			
$\frac{1}{2}^-$	179.9	168.7	~38[f]	0.90(5)
		152.6	~37[f]	0.88(6)
$\frac{5}{2}^-$	191.7	(11.8)	<1	
		164.4	~42[f]	0.66(4)
$\frac{9}{2}^-$	299.3	107.6	36(2)	0.63(4)
$\frac{13}{2}^-$	522.1	222.8	100(4)	0.81(3)
		185.5	2.7(3)	0.86(9)
$\frac{17}{2}^-$	858.5	336.4	99(4)	0.89(3)
		352.1	1.8(2)	
$\frac{21}{2}^-$	1296.6	438.1	94(4)	0.97(3)
$\frac{25}{2}^-$	1820.0	523.4	87(5)	1.04(3)
$\frac{29}{2}^-$	2412.3	592.3	79(4)	0.98(3)
$\frac{33}{2}^-$	3053.7	641.4	48(3)	1.12(4)
$\frac{37}{2}^-$	3663.1	609.4	37(3)	1.13(4)
		421.4	3.2(2)	
$\frac{41}{2}^-$	4230.7	567.6	22(1)	0.91(3)
$\frac{45}{2}^-$	4860.5	629.8	14.4(7)	1.07(6)
$\frac{49}{2}^-$	5556.6	696.1	9.4(5)	1.18(8)
$\frac{53}{2}^-$	6315.0	758.4	4.7(4)	1.2(1)
$(\frac{57}{2}^-)$	7128.6	813.6	2.8(4)	
$(\frac{61}{2}^-)$	7993.4	864.8	1.5(1)	
$(\frac{65}{2}^-)$	8913.0	919.6	<1	

TABLE I. *(Continued.)*

I^{π} [a]	E_{level} (keV)	E_{γ} (keV)[b]	I_{γ} [c]	Ang. Corr. Ratio
$(\frac{69}{2}^-)$	9886.6	973.6	<1	
$(\frac{73}{2}^-)$	10916.4	1029.8	<1	
$(\frac{77}{2}^-)$	(11992)	(1076)	<1	
	Band 5: [541]1/2 $\alpha = -1/2$			
$(\frac{3}{2}^-)$	348.1	168.2	<1	
$(\frac{7}{2}^-)$	468.4	120.3	1.4(2)	
		169.1	1.7(2)	
		276.7	3.8(3)	0.95(6)
$(\frac{11}{2}^-)$	723.3	254.9	10.2(7)	0.85(4)
		201.0	<1	
		216.7	1.4(1)	
		386.9	1.5(2)	
		424.0	8.7(6)	0.90(5)
$\frac{15}{2}^-$	1076.3	353.0	13.9(7)	0.99(5)
		554.1	6.9(5)	0.64(6)
$\frac{19}{2}^-$	1518.2	441.9	17(1)	0.97(3)
		660.1	6.0(4)	0.58(6)
$\frac{23}{2}^-$	2034.8	516.6	14(2)	0.75(4)[e]
		738.8	4.3(6)	
$\frac{27}{2}^-$	2602.3	567.5	12.2(7)	1.2(1)
		782.9	3.5(3)	
$\frac{31}{2}^-$	3152.0	549.7	8.3(6)	1.06(8)
		739.9	1.7(3)	
$\frac{35}{2}^-$	3620.0	468.0	4.9(3)	1.2(1)
$(\frac{39}{2}^-)$	4136.8	516.8	3.1(5)	
$(\frac{43}{2}^-)$	4728.3	591.5	2.6(3)	
$(\frac{47}{2}^-)$	5390.8	662.5	1.7(2)	
$(\frac{51}{2}^-)$	(6111)	(720)	<1	
	Band 6:			
$(\frac{25}{2}^-)$	2541.5	721.5	2.1(3)	
$(\frac{29}{2}^-)$	2851.4	309.9	1.3(2)	
		438.9	2.3(3)	
		1031.3	1.9(3)	
$\frac{33}{2}^-$	3241.7	390.3	3.1(4)	
		829.4	4.9(5)	1.0(1)
$\frac{37}{2}^-$	3795.1	553.4	4.3(4)	
		741.6	5.6(6)	1.1(1)[e]
$\frac{41}{2}^-$	4503.4	708.3	6.3(7)	1.1(1)
		(840)	<1	
$(\frac{45}{2}^-)$	5245.0	741.6	3.5(6)	
$(\frac{49}{2}^-)$	5987.7	742.7	1.7(4)	
	Band 7:			
$(\frac{21}{2}^-)$	2217.5	921.0	1.4(2)	
$(\frac{25}{2}^-)$	2623.2	405.7	1.2(2)	
		803.4	1.4(2)	
$(\frac{29}{2}^-)$	3074.5	451.3	3.9(5)	
		544.2	2.4(3)	
		662.2	6.6(7)	

TABLE I. *(Continued.)*

I^{π} [a]	E_{level} (keV)	E_{γ} (keV)[b]	I_{γ} [c]	Ang. Corr. Ratio
$(\frac{33}{2}^-)$	3622.0	547.5	3.9(5)	
		568.1	1.2(2)	
$(\frac{37}{2}^-)$	4225.0	603.0	4.2(5)	
$(\frac{41}{2}^-)$	4883.5	658.5	2.1(3)	
$(\frac{45}{2}^-)$	5591.8	708.3	1.4(2)	
	Band 8: [514]9/2 $\alpha = +1/2$			
$\frac{9}{2}^-$	219.4	123.0	N/D	0.79(5)
$\frac{13}{2}^-$	506.4	287.0	24(2)	1.2(1)
		170.2	92(4)	0.75(3)
$\frac{17}{2}^-$	924.5	418.1	59(3)	0.97(3)
		232.4	70(3)	0.85(4)
$\frac{21}{2}^-$	1430.2	505.7	69(3)	0.87(4)
		280.1	57(2)	0.82(5)
$\frac{25}{2}^-$	1994.3	564.1	60(2)	0.96(6)
		311.5	41(2)	0.82(4)
$\frac{29}{2}^-$	2570.8	576.5	53(2)	1.06(5)
		309.0	32(2)	0.72(4)
$\frac{33}{2}^-$	3003.4	432.6	19(1)	0.92(5)
		207.9	42(4)	0.68(4)[e]
$\frac{37}{2}^-$	3440.1	436.7	17(1)	1.03(7)
		229.6	33(2)	0.72(5)
$\frac{41}{2}^-$	3974.1	534.0	13(2)	0.96(6)[e]
		275.4	20(1)	0.75(5)
$\frac{45}{2}^-$	4601.5	627.4	11.4(7)	1.3(1)
		319.8	10.4(6)	0.65(4)
$\frac{49}{2}^-$	5305.6	704.1	7.7(4)	0.96(5)
		358.8	6.2(3)	0.61(5)
$(\frac{53}{2}^-)$	6073.8	768.2	4.1(2)	
		394.6	2.7(2)	
$(\frac{57}{2}^-)$	6901.1	827.3	3.3(1)	
$(\frac{61}{2}^-)$	7789.7	888.6	1.8(1)	
$(\frac{65}{2}^-)$	8745.3	955.6	<1	
	Band 8: [514]9/2 $\alpha = -1/2$			
$\frac{11}{2}^-$	336.3	116.9	~62[d]	0.67(2)
$\frac{15}{2}^-$	692.2	355.9	46(2)	0.94(2)
		185.6	83(3)	0.74(2)
$\frac{19}{2}^-$	1150.4	458.2	90(3)	0.93(3)
		225.6	58(4)	0.74(2)[e]
$\frac{23}{2}^-$	1683.0	532.6	82(5)	1.02(2)[e]
		252.4	46(2)	0.76(3)
$\frac{27}{2}^-$	2262.0	579.0	75(3)	1.00(3)
		267.4	31(2)	0.69(3)
$\frac{31}{2}^-$	2795.3	533.3	60(4)	1.02(2)[e]
		224.6	33(4)	0.74(2)[e]
$\frac{35}{2}^-$	3210.6	415.3	24(1)	1.07(4)
		206.9	40(5)	0.68(2)[e]
$\frac{39}{2}^-$	3698.6	488.0	19(1)	1.1(1)
		258.0	27(2)	0.71(3)

TABLE I. *(Continued.)*

I^{π} [a]	E_{level} (keV)	E_{γ} (keV)[b]	I_{γ} [c]	Ang. Corr. Ratio
$\frac{43}{2}^-$	4281.6	583.0	16(2)	0.97(4)
		307.4	13.9(7)	0.72(2)
$\frac{47}{2}^-$	4946.7	665.1	7.9(5)	1.2(1)
		345.4	7.6(5)	0.55(4)
$(\frac{51}{2}^-)$	5679.1	732.4	5.6(3)	
		373.4	3.1(2)	
$(\frac{55}{2}^-)$	6467.5	788.4	3.3(2)	
$(\frac{59}{2}^-)$	7309.8	842.3	3.1(2)	
$(\frac{63}{2}^-)$	8207.0	897.2	1.4(1)	
$(\frac{67}{2}^-)$	9158.1	951.1	<1	
$(\frac{71}{2}^-)$	10154.7	996.6	<1	

[a]Spin and parity of the depopulated state.
[b]Uncertainties in the quoted γ-ray energies are 0.2 keV for most transitions; for relatively weak transitions (<1), 0.5 keV uncertainties are appropriate.
[c]Relative intensity of the transition with respect to the intensity of the 222.8-keV transition in Band 5.
[d]Estimate based on intensity balance and branching ratio.
[e]Unresolved doublet.
[f]Estimate based on intensity balance.

$\alpha = -1/2$ signature to high spin ($I = 55/2$). The extension of the $\alpha = +1/2$ sequence above the 25/2 state proved to be more challenging. A spectrum of γ rays in coincidence with the states above the 29/2 level of this sequence is given in Fig. 3(c). It is evident from this spectrum that this structure favors feeding bands 1 (through the 582- and 306-keV transitions) and 4 (through the 377-keV transition) in comparison with the tentative 454-keV inband transition. Indeed, one may note the numerous linking transitions between all four positive-parity bands near $I = 29/2$ in Fig. 1. Inspection of Fig. 4(a) reveals that all four $29/2^+$ states lie within 110 keV of each other, and, thus, significant mixing may be expected. Moreover, this is also at the point where all four bands undergo the lowest neutron alignment (see below).

C. Band 3

A new decoupled structure that decays to three different bands was observed and is labeled as band 3 in Fig. 1.

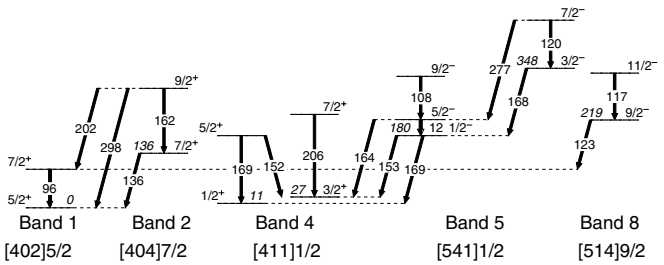

FIG. 2. Partial level scheme for ^{169}Ta highlighting the low-spin portion of the diagram. Bandhead excitation energies are shown in italics.

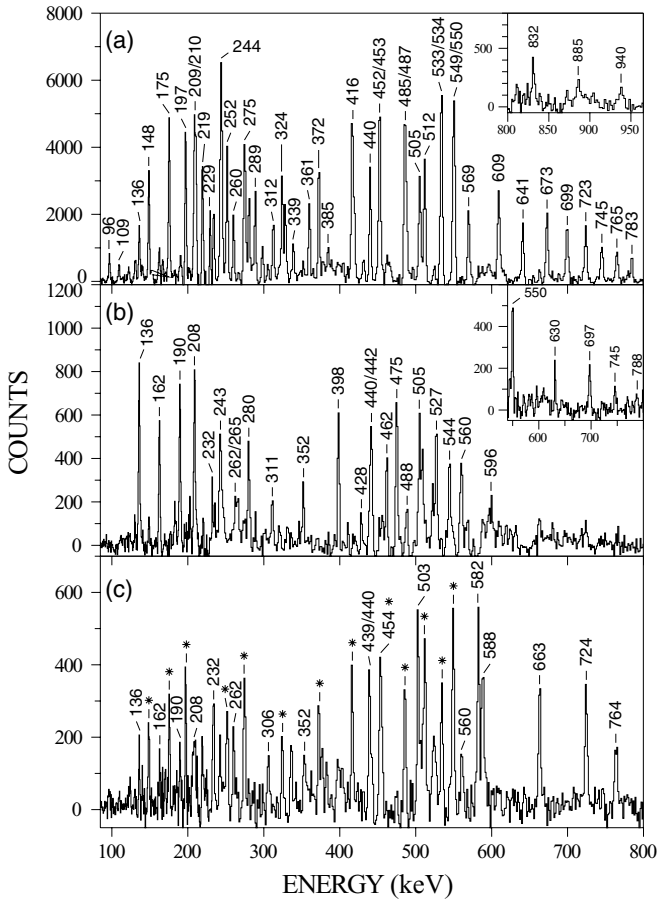

FIG. 3. Representative coincidence spectra for bands 1 and 2. Unless otherwise indicated, the spectra provided are the result of a sum of all triple coincidence gates using $E2$ transitions. (a) Spectrum of band 1 ([402]5/2); inset displays the highest energy γ rays observed in the $\alpha = +1/2$ sequence. (b) Spectrum of band 2 ([404]7/2), where all combinations of triple gates of $E2$ transitions were used up to the $29/2^+$ state; high-energy inset displays the extension of the $\alpha = -1/2$ sequence, which was produced with all possible triple gates of $E2$ transitions above the $27/2^+$ state. (c) Spectrum of the high-energy portion of the $\alpha = +1/2$ sequence of band 2; all combinations of inband $E2$ transitions above the $29/2^+$ state were used to produce this spectrum. Asterisks denote coincident transitions from band 1.

Figure 5(a) displays the coincidence of band 3 with the $\alpha = +1/2$ signature of band 4. The angular correlation ratios of the 417- and 508-keV linking transitions [0.95(4) and 1.0(1), respectively] are consistent with these γ rays being of stretched $E2$ character. Thus, a confident spin/parity assignment can be made for this band, where the lowest and highest spin states are found to have the $21/2^+$ and $65/2^+$ quantum numbers, respectively. In addition, eight other decay-out transitions are found throughout a large spin range (21/2–37/2).

D. Band 4

Band 4 was previously observed up to $I = 39/2$ and assigned positive parity in Refs. [13,19]. The present data allowed for the extension of the $\alpha = -1/2$ sequence to 55/2,

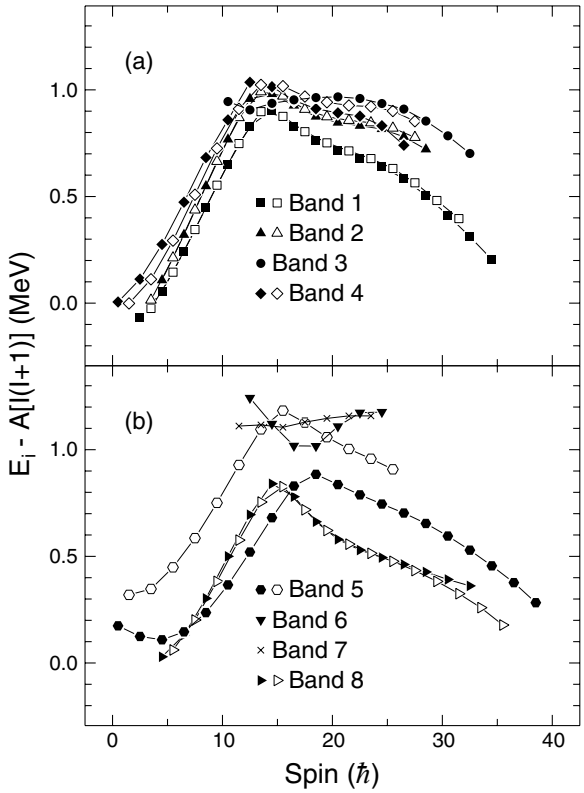

FIG. 4. Excitation energies of the observed levels minus a rigid-rotor reference, where this reference was assumed to have a moment of inertia parameter $A = 0.0077$ MeV. Positive (negative) signatures are represented with filled (open) symbols.

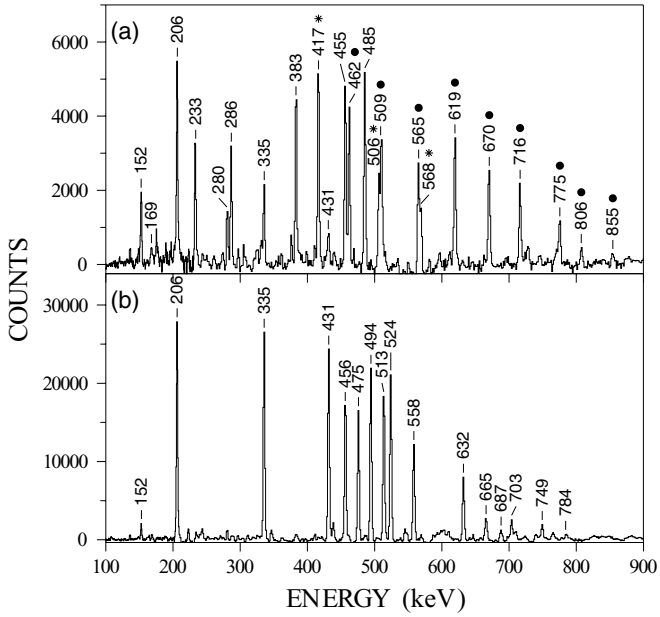

FIG. 5. (a) Spectrum of band 3 ([660]1/2) and the $\alpha = +1/2$ sequence of band 4 ([411]1/2). All combinations of $E2$ transitions above the 5/2 level within both bands were used to produce the spectrum. Solid circles denote γ rays originating from band 3 (b) Sample coincidence spectrum of the $\alpha = -1/2$ signature for band 4. All combinations of triple gates with inband transitions produced this spectrum.

and a supporting spectrum is provided in Fig. 5(b). The signature partner was also extended to $53/2^+$, despite the strong loss in intensity due to the decay out at $I = 33/2$ to band 3 through the 506-keV linking transition (see Fig. 1). In fact, the $33/2^+$ states of these two bands are only separated by 3 keV. Therefore, the 546-, 411-, and 428-keV inband transitions between $I = 21/2$ and $I = 33/2$ are found to be quite weak. Linking transitions were also found from band 4 to band 5, which thus provides a connection between the positive- and negative-parity structures. The electromagnetic nature of these transitions feeding band 5 could not be determined from the present data. However, the deduced configuration assignments for bands 4 and 5 ([411]1/2 and [541]1/2, respectively, see Ref. [13] and below) suggest that these are $E1$ linking transitions. Indeed, a comparable decay pattern is observed between two similar structures in ^{171,173}Ta [9,22], giving further confidence in the assignment. At higher spins, a short sequence of γ rays is found to decay into the $\alpha = -1/2$ sequence at $I = 43/2$.

E. Band 5

Only the $\alpha = +1/2$ sequence of band 5 was previously observed by Li *et al.* [13]. Negative parity was assigned to this sequence because it was interpreted as being based on the [541]1/2 orbital [13]. In addition, lifetime measurements based on the 153- and 169-keV lines decaying near the bottom of the band suggested that this sequence is based on an isomeric state with a half-life of 17(4) ns [20]. These transitions are observed in the sample spectrum provided in Fig. 6(a), along with a 164-keV γ ray that is in coincidence with all of the inband transitions of band 5. However, these three transitions are not in coincidence with each other. The fact that the 153- and 169-keV transitions display the same half-life indicates that they decay from the same state. The delayed spectrum of Fig. 1 in Ref. [20] shows the 153- and 169-keV γ rays clearly, but it has little evidence for the 164-keV line. Therefore, the 164-keV transition likely decays from a separate level with respect to the other two γ rays. Only the bandhead state would have a greater than 1 ns lifetime; thus, the 153- and 169-keV lines are assumed to depopulate the $1/2^-$ state and feed the $3/2^+$ and $1/2^+$ levels of band 4 (see Fig. 2). The latter two states in band 4 are separated by 16 keV, which agrees well with the energy difference of the 153- and 169-keV transitions. This assignment also requires that both γ rays be of unstretched $E1$ character, and indeed, the angular correlation ratios for both transitions are approximately 0.9 (see Table I), which is consistent with unstretched dipoles. A bandhead energy of 180 keV is then determined for band 5. Note that the $1/2^-$ assignment is different from that given in Ref. [20], where the authors assumed the bandhead to have $5/2^-$ quantum numbers. Evidence that the 164-keV line actually depopulates the $5/2^-$ member of this band is given below.

Since the 164-keV transition was not observed in the delayed spectrum of Ref. [20], it is likely associated with a prompt decay, which suggests that another level lies above the $1/2^-$ bandhead state. The angular correlation ratio of 0.66(4) indicates that this transition is a pure stretched dipole;

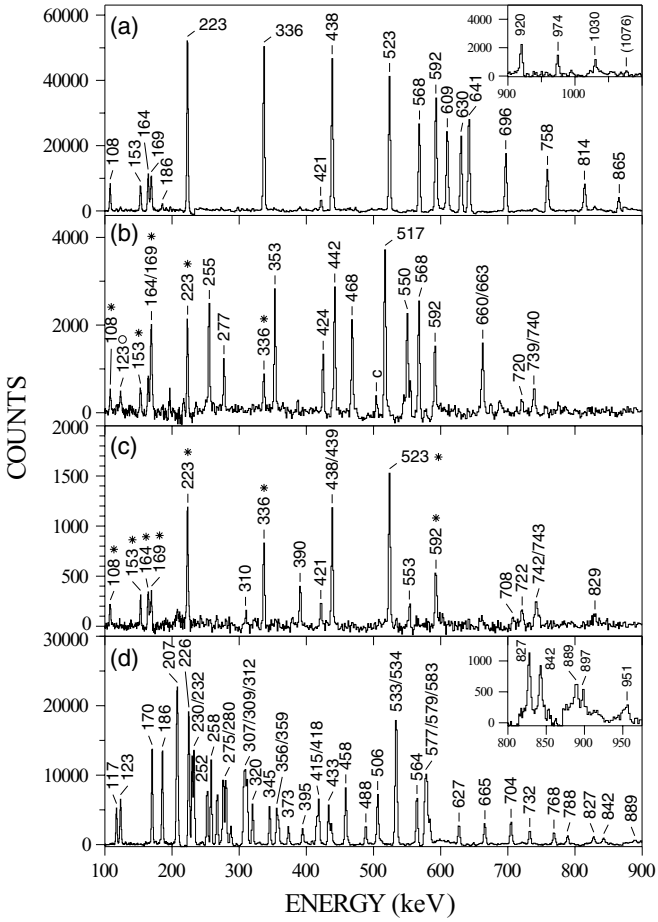

FIG. 6. (a) Spectrum of the $\alpha = +1/2$ sequence of band 5 produced by summing all triple coincidence gates where two transitions were below the 37/2 state and one was above this level. High-energy γ rays are given in the inset. (b) Transitions belonging to the $\alpha = -1/2$ sequence of band 5. Lines marked with an asterisk or a circle are from the favored signature of bands 5 and 8, respectively. (c) Sample spectrum displaying the γ rays of band 6. This spectrum results from summing triple coincidence gates where two gating energies come from the list of 108, 223, 336, and 438 keV (from band 5), and the third gating energy was either the 310, 390, or 553 keV line in band 6. Asterisks denote transitions from band 5. (d) Spectrum of band 8 resulting from the summation of all possible triple-gate combinations on the inband $\Delta I = 1$ transitions. High-energy γ rays are displayed in the inset.

therefore, the 164-keV γ ray is assigned as the decay from the $5/2^-$ state in band 5 to the $3/2^+$ state in band 4. This requires the presence of a 12-keV transition between the $5/2^-$ and $1/2^-$ states (as shown in Fig. 2) which is below the detection threshold of the Gammasphere detectors. However, confirmation of this assignment is found from the decay of the newly observed signature partner of band 5.

A spectrum of the unfavored $\alpha = -1/2$ sequence is displayed in Fig. 6(b). Angular correlation ratios (see Table I) indicate that the 424-, 554-, and 660-keV lines are of mixed $M1/E2$ character, thus confirming the spin assignments proposed in Fig. 1. The 169-keV line is found to be self-coincident when double gated with the 120-keV transition that feeds the $3/2^-$ state. This suggests a 168-keV transition from the $3/2^-$ to the $1/2^-$ level, where the $1/2^-$ level has an excitation energy of 180 keV (see Fig. 2), which is consistent with our placement of the $1/2^-$ level. In addition, the 277-keV line from the $7/2^-$ state of the $\alpha = -1/2$ sequence must feed the $5/2^-$ state as it is in coincidence with the 153-, 164-, and 169-keV transitions. This requires the $5/2^-$ level to be located at an energy of 192 keV. Therefore, it appears that both the $1/2^-$ and $5/2^-$ states have been observed and that the $5/2^-$ level lies 12 keV higher than the $1/2^-$ bandhead. This low-energy $5/2^-$ to $1/2^-$ transition is consistent with that seen in similar bands of ^{167}Lu (15 keV) [23], ^{165}Tm (23 keV) [24] and ^{163}Ho (29 keV) [25], which are isotones of ^{169}Ta.

Li *et al*. [13] stated that they observed the favored signature of band 5 up to spin 73/2; however, two of the inband transitions were improperly associated with this sequence. The 742- and 740-keV transitions were previously assigned as depopulating the 53/2 and 61/2 states, respectively. The coincidence spectrum displayed in Fig. 6(a) provides no evidence of these transitions. This spectrum was produced by summing all combinations of triple coincidence gates of two transitions below the 37/2 state with one transition above the same state. If the 742- and 740-keV lines were members of this sequence, peaks would be evident in the spectrum. Their absence invalidates their placement in Ref. [13], and it was determined that these transitions are actually part of band 6, which is discussed below. Figure 6(a) also displays how band 5 could be extended to 77/2, the highest spin state observed in this nucleus. Although this sequence displays large signature splitting [see Fig. 4(b)], the unfavored sequence was observed up to 51/2, as shown in the sample spectrum of Fig. 6(b).

F. Band 6

Band 6 is a new structure that strongly feeds band 5 through a series of linking transitions seen in Fig. 1. The 829-keV linking transition from band 6 likely has an $E2$ nature, as the angular correlation ratio was determined to be 1.0(1). Therefore, the spins and negative parity of the members of this sequence can be assigned as given in Fig. 1. Three transitions with energies near 742 keV are found to be part of this structure or of the decay to band 5. Thus, it is likely these transitions are those that were mistakenly placed in band 5 by Li *et al*. [13]. A sample spectrum is given in Fig. 6(c). Note that a relatively strong linking transition from the 37/2 state of band 5 (421 keV) is found decaying to band 6, indicating a strong interaction between the bands even though the states are separated by over 150 keV.

G. Band 7

No reliable angular correlation ratios could be determined for the linking transitions of the new sequence labeled as band 7 in Fig. 1. As a result, a number of other considerations were used to arrive at the proposed quantum numbers. The fact that the third lowest state in the sequence decays to a $29/2^-$ level in band 5 and a $27/2^+$ level in band 4 helps to limit the choices for possible spin assignments. If positive parity is assumed, the spin of the lowest state is most likely $I = 23/2$ such that the linking transitions to band 5 are of stretched

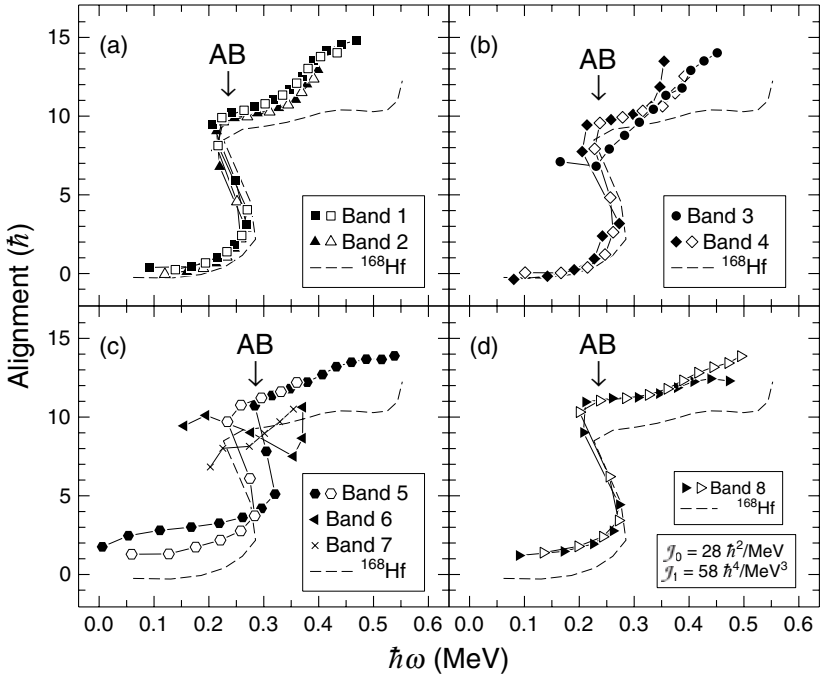

FIG. 7. Alignments for the bands in ^{169}Ta. Harris parameters of $\mathcal{J}_0 = 28\hbar^2$/MeV and $\mathcal{J}_1 = 58\hbar^4$/MeV^3 were used to subtract the angular momentum of the rotating core. Observed *AB* neutron crossings are designated. Filled (empty) symbols denote $\alpha = +1/2$ $(-1/2)$ sequences.

$E1$ character and the 544-keV linking transition with band 4 corresponds to a stretched $E2$ transition. On the other hand, if band 7 has negative parity, a spin of 21/2 for the lowest observed state is likely and the 544-keV line becomes a stretched $E1$ transition. In Fig. 4(b), band 7 is shown assuming the 23/2 spin assignment, and it is found to have similar energies as band 6. A 21/2 spin assignment pushes band 7 up in energy by ~300 keV with respect to the position given in the figure. Noting that the intensities of bands 6 and 7 are similar (see Table I) and assuming statistical feeding leads to the conclusion that the bands are likely to have similar excitation energies. For this reason, the $23/2^+$ spin/parity assignment is preferred and tentatively given to the lowest state of band 7. In addition, with this spin assignment, one may infer that the $I = 35/2$ states of bands 5 and 7 are nearly degenerate [see Fig. 4(b)], but they do not interact. Such a behavior suggests that the two bands have opposite parities, as proposed in Fig. 1.

H. Band 8

Finally, the sequence labeled band 8 in Fig. 1 is found to be the yrast sequence for most of the observed spin range, as seen in Fig. 4(b). Li *et al.* [13] observed this strongly coupled sequence up to spin 59/2 and assigned negative parity based on the proposed configuration. Zhang *et al.* [20] determined that a 123-keV transition linked the bandhead state with the 96-keV $7/2^+$ level in band 1, and they measured a 28(5) ns lifetime for the resulting 219-keV state. An angular correlation ratio of 0.79(5) was measured for this 123-keV line, which is larger than expected for an $E1$ transition. However, the relatively long lifetime of the 9/2 level will cause a dealignment and thus skew the angular correlation results. The angular correlation ratio of 0.86(9) for the 186-keV line decaying from the $13/2^-$ level in band 5 to the 336-keV state in band 8 indicates that it is a mixed $M1/E2$ transition. Therefore, this level is likely $11/2^-$ and is consistent with the 219-keV state having $9/2^-$. The spectrum provided in Fig. 6(d) displays the transitions that allowed the extension of the structure to 71/2.

IV. DISCUSSION

With a predicted deformation of $\beta_2 = 0.22$–0.25 [13,14], the proton Fermi surface for ^{169}Ta is expected to be near a host of Nilsson orbitals. Indeed, Ref. [14] predicts six bandhead states to be below 500 keV. These orbitals include the $d_{5/2}[402]5/2$, $g_{7/2}[404]7/2$, $h_{11/2}[514]9/2$, $h_{9/2}[541]1/2$, and $d_{3/2}[411]1/2$ states. In addition, the $i_{13/2}[660]1/2$ level is known to approach the yrast line at medium spins in ^{171}Ta [7–9]. Configurations of the bands in ^{169}Ta are assigned below based on the structures seen in nearby nuclei and on the intrinsic properties of the bands. In particular, plotting the alignment of the bands versus rotational frequency (Fig. 7) was useful for these assignments. Harris parameters of $\mathcal{J}_0 = 28\hbar^2$/MeV and $\mathcal{J}_1 = 58\hbar^4$/MeV^3 were chosen such that the ground-state band in the neighboring even-even nucleus ^{168}Hf [26] has nearly zero initial alignment and has a constant alignment above the first crossing. This sequence is shown for comparison in each of the four panels of Fig. 7.

A. Band 1: The [402]5/2 structure

The initial alignment of band 1 in Fig. 7(a) is small, which is typical for a structure associated with a relatively high-K configuration. In addition, its strongly coupled nature is also consistent with the assignment originally proposed by Li *et al.* [13] as the [402]5/2 orbital for this sequence. Although we are in agreement with the interpretation that band 1 is predominantly based on this orbital, the measured $B(M1)/B(E2)$ ratios indicate a strong mixing with another configuration. Figure 8(a) displays these ratios for bands 1 and 2; note that both structures have very similar values below $I = 25/2$. Theoretical $B(M1)$ values were calculated using the geometric

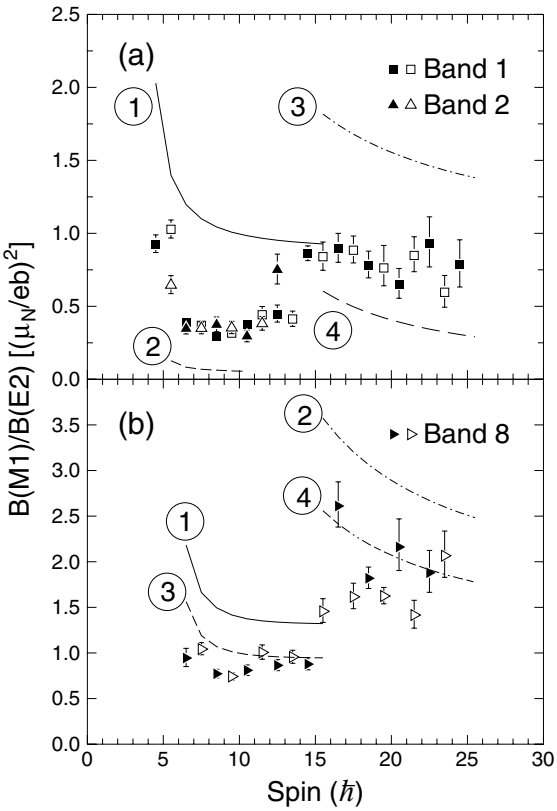

FIG. 8. Measured $B(M1)/B(E2)$ ratios for bands 1, 2, and 8 in ^{169}Ta. Filled (empty) symbols represent the experimental values for the $\alpha = +1/2$ $(-1/2)$ sequence. Theoretical calculations are displayed as lines with the following configurations. (a) 1: $\pi d_{5/2}[402]5/2$; 2: $\pi g_{7/2}[404]7/2$; 3: $\pi d_{5/2}\nu AB$; 4: $\pi g_{7/2}\nu$ AB. (b) 1: $h_{11/2}[514]9/2$; 2: $\pi h_{11/2}\nu AB$; 3: $\pi h_{11/2}$ with $Q_0 = 6.5$ b; 4: $\pi h_{11/2}\nu AB$ with $Q_0 = 6.5$ b.

model of Dönau [27] with $g_R = Z/A$ and the g_Ω values given in Table II of Ref. [9]. The standard rotational form of the $B(E2)$ strength [28] was calculated assuming a quadrupole moment of 5.5 b deduced from the predicted deformation of $\beta_2 = 0.22$ [14]. The theoretical $B(M1)/B(E2)$ ratios for different configurations are displayed as different lines in Fig. 8. Neither calculated values for the [402]5/2 (line 1) nor the [404]7/2 (line 2) configurations satisfactorily reproduce the $B(M1)/B(E2)$ ratios of bands 1 and 2. Indeed, the experimental values for both structures lie between these two calculated ratios. In view of this observation, bands 1 and 2 should both be interpreted as having significant components of the [402]5/2 and [404]7/2 orbitals in their respective wave functions. As these configurations are pseudospin partners [29], it is not necessarily surprising that such strong mixing occurs.

A backbend in the alignment plot [Fig. 7(a)] is observed at a frequency of 0.242 MeV with an alignment gain of approximately $10.5\hbar$. These values (frequency and alignment) are similar to those of the first crossing in the ground-state band of ^{168}Hf (0.261 MeV and alignment gain of $\sim 9.5\hbar$). The first crossing in this region is well documented to result from the alignment of the lowest $i_{13/2}$ quasineutrons and is commonly called the AB crossing [30]. Note that the interaction strength of this AB alignment is remarkably similar for the [402]5/2 band and the ground-state band in ^{168}Hf. Above this crossing, significant mixing between the [402]5/2 and [404]7/2 configurations appears to persist, based on the measured $B(M1)/B(E2)$ ratios of band 1 [Fig. 8(a)]. Above the AB crossing ($I > 29/2$), the measured ratios continue to lie between the theoretical values for the $\pi d_{5/2}\nu$ AB (line 3) and $\pi g_{7/2}\nu AB$ (line 4) configurations.

Cranked shell model (CSM) calculations were performed in order to help interpret the observed crossings. However, in this mass region, the CSM has consistently predicted a lower crossing frequency for the AB alignment by $\sim$45 keV [10] when using the BCS treatment for pairing. A possible explanation for this discrepancy is that the assumed pairing field is too small. The neutron pairing energy can alternatively be estimated from the mass differences of neighboring nuclei, as adopted in Ref. [31]. By using the five-point fit defined in Ref. [32], a pairing energy of 1.22 MeV was determined, a value $\sim$20% larger than the BCS one. Incorporating this value into the CSM produced the quasineutron Routhian diagram of Fig. 9(a). The AB crossing is now predicted to occur near

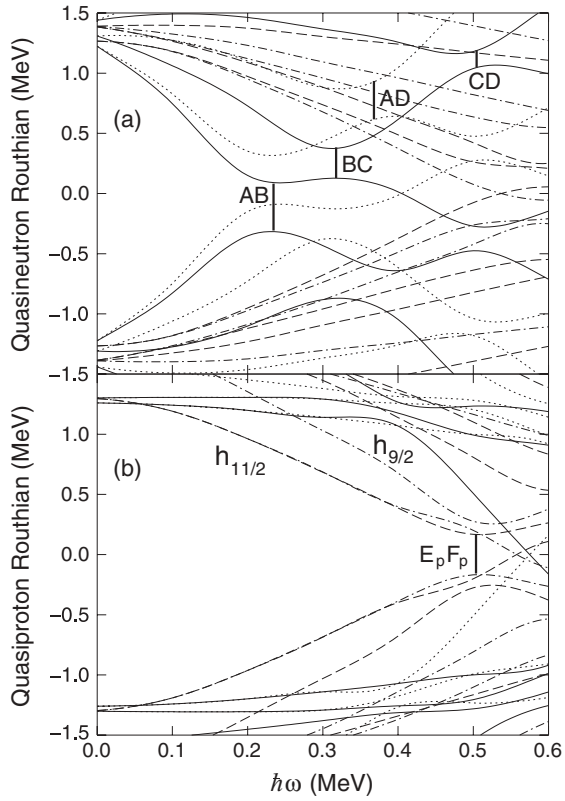

FIG. 9. Quasiparticle Routhians for ^{169}Ta calculated with the CSM. Deformation parameters of $\beta_2 = 0.22$, $\beta_4 = 0$, and $\gamma = 0$ were assumed. Pairing energy was determined from experimental masses using the five-point fit procedure as described in Ref. [32]. Line types are defined as follows: solid (positive parity, $\alpha = +1/2$), dotted (positive parity, $\alpha = -1/2$), dashed (negative parity, $\alpha = -1/2$), and dash-dot (negative parity, $\alpha = +1/2$). (a) Pairing energy of $\Delta_n = 1.22$ MeV was assumed; predicted crossings are displayed. (b) Pairing energy of $\Delta_p = 1.26$ MeV was assumed; first proton crossing is also indicated.

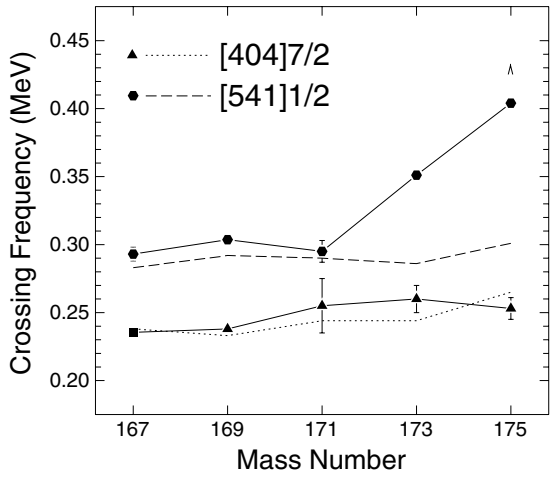

FIG. 10. Experimental *AB* crossing frequencies for the [404]7/2 and [541]1/2 bands in Ta isotopes. Note that the square shown for ^{167}Ta is the crossing frequency observed in the [402]5/2 band. Dotted and dashed lines represent the CSM calculated crossing frequencies for these configurations when an empirical pairing strength was employed, see text for details.

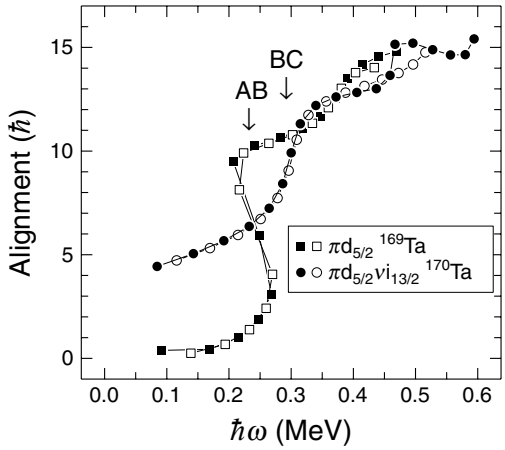

FIG. 11. Alignment of $\pi d_{5/2}$ and $\pi d_{5/2}\nu i_{13/2}$ bands in ^{169}Ta and ^{170}Ta, respectively. The same Harris parameters were used as in Fig. 7.

0.23 MeV, in better agreement with the data. To test the validity of this method, the empirical pairing energies were calculated for the $^{167-175}$Ta isotopes, and CSM calculations were performed using the deformation parameters defined in Ref. [14]. A comparison of the predicted and experimental *AB* crossings for the [404]7/2 band[1] can be found in Fig. 10. Good agreement is systematically observed for the [404]7/2 band; therefore, the empirical pairing energy appears to provide a better estimate of the actual pairing strength.

A new crossing at 0.37 MeV can be observed in Fig. 7(a) for band 1. Note that a similar crossing is found in bands 2 and 4 [Figs. 7(a) and 7(b), respectively]. These two structures have been associated with the [404]7/2 and [411]1/2 orbitals, respectively (see below). Cranked shell model calculations suggest that the E_pF_p (alignment of $h_{11/2}$ protons) or the *CD* (alignment of the third and fourth $i_{13/2}$ neutrons) are the next available crossings. However, both of these crossings are predicted to occur near 0.5 MeV, as seen in Fig. 9. Note that the proton pairing energy was empirically derived in a similar manner as the neutron pairing discussed above. With such a large discrepancy between the observed and predicted crossing frequencies, the alignment profiles of neighboring nuclei must be inspected to gain further insight into the nature of this crossing.

The *CD* crossing is clearly observed in ^{166}Hf [33] at 0.42 MeV and then followed by the E_pF_p alignment at 0.5 MeV. As seen in Fig. 7(a), the *CD* crossing is not readily seen in ^{168}Hf, although the small interaction near 0.4 MeV could possibly be associated with this alignment. The upbend at 0.55 MeV is likely associated with the proton crossing similar to the observations in ^{166}Hf and the CSM prediction shown in Fig. 9(b). Data on the neighboring odd-odd ^{170}Ta nucleus were obtained in the present experiment [34], and the resulting alignment for the $\pi d_{5/2}\nu i_{13/2}$ band is plotted with the $\pi d_{5/2}$ band of ^{169}Ta in Fig. 11. The *AB* crossing is Pauli blocked in ^{170}Ta as the *A* orbital is already occupied. Therefore, the *BC* alignment is seen at 0.3 MeV, which is in good agreement with the CSM calculations [Fig. 9(a)]. However, there is no crossing at 0.37 MeV in this band. If the alignment at 0.37 MeV in the $\pi d_{5/2}$ band of ^{169}Ta were the result of the E_pF_p crossing, the same alignment ought to be observed in the $\pi d_{5/2}\nu i_{13/2}$ sequence in ^{170}Ta. On the other hand, the *CD* crossing would be blocked in the $\pi d_{5/2}\nu i_{13/2}$ band following the *BC* alignment. Therefore, the crossing at 0.37 MeV appears to be best associated with the *CD* interpretation. A reduction in neutron pairing is expected following the *AB* crossing; thus, the pairing used in Fig. 9(a) is too large, which can account for the discrepancy between the data and the calculations. For the CSM to reproduce the *CD* crossing near 0.4 MeV, the pairing field must be reduced by at least 50%. A 40% reduction of pairing was used in Ref. [35] to reproduce the *CD* crossing frequency at 0.38 MeV in ^{171}Re, an isotone of ^{169}Ta. It is interesting to note that there is no clear sign of the *CD* crossing in the $N = 98$ nuclei ^{170}Hf [36] and ^{171}Ta [9]. This suggests that the location and the interaction strength of the *CD* alignment are strongly dependent on the neutron Fermi level and deserves further investigation in future studies.

B. Band 2: The [404]7/2 structure

As previously stated, band 2 is a newly observed sequence that interacts strongly with the [402]5/2 structure. This strongly coupled sequence has an alignment profile that is nearly identical to that of band 1 [see Fig. 7(a)]. The *AB* crossing is observed at 0.238 MeV, and a second alignment found near 0.37 MeV is likely the *CD* crossing. Two strongly coupled, positive-parity sequences with similar characteristics are commonly seen in Ta nuclei, where one is based on the [402]5/2 orbital, and the other on the [404]7/2 state. Given that the bandhead state of band 2 has the quantum numbers $7/2^+$,

[1]The [404]7/2 band was chosen because the [402]5/2 sequence has not been extended through this crossing in ^{173,175}Ta.

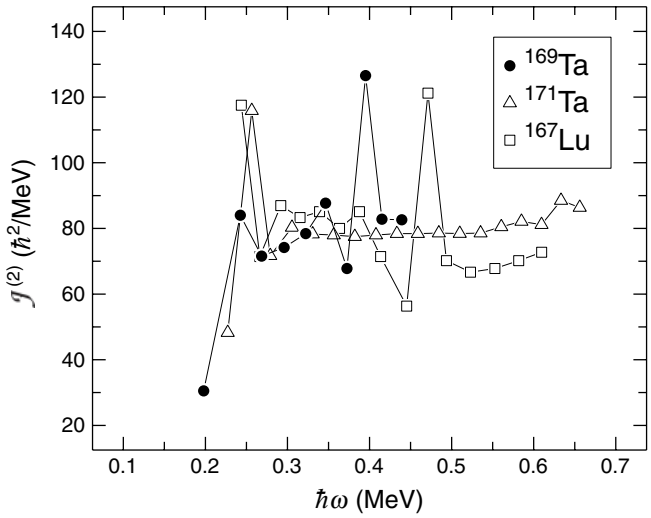

FIG. 12. Dynamic moments of inertia of the $\pi i_{13/2}$ bands in ^{169}Ta, ^{171}Ta, and ^{167}Lu.

this sequence is assigned as the band primarily based on the [404]7/2 orbital. As stated above, the $B(M1)/B(E2)$ values of band 2 [Fig. 8(a)] are greater than the theoretical values, indicating substantial mixing with the [402]5/2 sequence.

C. Band 3: The [660]1/2 structure

The fact that band 3 is decoupled suggests that it is based on a low-K orbital. The excitation energy of the bandhead state is at a relatively high energy as compared with the others, since this sequence is only observed down to the 21/2 level at 1875.1 keV. A decoupled sequence has been observed in ^{171}Ta [7–9] as well as ^{167}Lu [5], and in those two cases, the decay to the other bands occurs near 25/2; i.e., the situation is similar to that of band 3. Both of these latter two structures have been associated with the $i_{13/2}$[660]1/2 orbital and display large dynamic moments of inertia, presumably because of an enhanced deformation with respect to the other bands. The dynamic moment of inertia $J^{(2)}$ of band 3 is presented along with that of the ^{171}Ta and ^{167}Lu $i_{13/2}$ bands in Fig. 12. Although there is some fluctuation in the $J^{(2)}$ values for band 3, it is clear that they are of the same average magnitude as those of the previously known $i_{13/2}$ structures. On the basis of those observations, band 3 is assigned as the [660]1/2 sequence in ^{169}Ta. The alignment profile of this band is given in Fig. 7(b) where it appears to steadily gain alignment throughout the observed frequency range. This is consistent with the profile observed for the $i_{13/2}$ band in ^{171}Ta [9]. As discussed in Ref. [9], it is possible that this is due to an AB crossing with a very large interaction strength resulting from the enhanced deformation.

The $i_{13/2}$ band has attracted substantial interest in this region as wobbling bands based on this orbital have been identified in ^{161,163,165,167}Lu [1,4–6]. Identification of a wobbling sequence is unique to a nucleus with stable triaxial deformation. Indeed, one of the main objectives of this experiment was to search for a wobbling band in ^{171}Ta and its neighbors. No sequence with the characteristics of wobbling could be observed in ^{171}Ta or ^{169}Ta. However, since ^{169}Ta was not the main product of this reaction, it is possible that this collective mode exists, but it is either not fed or fed too weakly with the present reaction; so a dedicated experiment for ^{169}Ta may be necessary to search for this exotic structure.

D. Band 4: The [411]1/2 structure

Li *et al.* [13] associated band 4 with the [411]1/2 orbital. The significant signature splitting observed for band 4 in Fig. 4(a) is consistent with this low-K assignment. The alignment for this sequence is given in Fig. 7(b), and little initial alignment is present, an observation in line with a band based on a $d_{3/2}$ orbital. Therefore, we agree with Li *et al.* and associate band 4 with the [411]1/2 orbital. The first and second crossings are similar to those observed in bands 1 and 2; thus, the same interpretations are given for these alignments.

E. Band 5: The [541]1/2 structure

The favored $\alpha = +1/2$ signature of band 5 was previously identified and assigned to the [541]1/2 configuration [13]. The relatively high initial alignment of $\sim 3\hbar$ seen in Fig. 7(c) and the delayed AB crossing at 0.30 MeV are indeed characteristic of this orbital [10]. A new sequence is found to strongly decay into this band and is interpreted as the unfavored signature partner of the same [541]1/2 band. At low frequencies, the unfavored sequence has $\sim 1.7\hbar$ less alignment than the favored one. Such behavior is predicted by the CSM for unfavored signatures resulting from high-j, low-K orbitals. However, the $\alpha = -1/2$ structure undergoes the AB alignment at 0.26 MeV, i.e., with only a small delay with respect to the other bands. A similar difference in crossing frequencies between the signature partners of the [541]1/2 band is found in ^{173}Ta [22]. The delay of the AB alignment in the favored sequence is thought to be the result of the larger deformation combined with the proton-neutron (p-n) interaction between the $h_{9/2}$ proton and the $i_{13/2}$ neutron [10]. Figure 10 compares experimental crossing frequencies with those from CSM calculations utilizing the empirically derived pairing energy and enhanced deformation parameter predicted for the [541]1/2 orbital [14]. Good agreement is found for $^{167-171}$Ta, while large deviations are observed in the heavier Ta nuclei. Perhaps this suggests that the p-n interaction plays a small role in the $N < 100$ Ta nuclei but becomes more prominent and is responsible for the large delays seen in the $N \geqslant 100$ Ta isotopes. The fact that a smaller delay is evident in the unfavored sequence may imply signature dependent deformation and/or p-n interaction. If only deformation is considered, the CSM suggests that the unfavored signature has a deformation 20% smaller than the favored sequence. There is a steady gain of alignment above the AB crossing [Fig. 7(c)], which may indicate that the CD crossing occurs as in the positive-parity bands, but with larger interaction strength. A difference in deformation can alter interaction strengths as pointed out in Ref. [37], but the alignment gain in band 5 appears to be similar to those found in the positive-parity bands.

F. Band 6

Inspection of Fig. 4(b) indicates that band 6 experiences a strong interaction with the [541]1/2 sequence, as the two bands appear to repel each other near $I = 35/2$. Such a strong interaction suggests that the two bands have very similar wave functions. Therefore, at low spin, we assign band 6 as the S band ($\pi h_{9/2}\nu$ AB); and at high spin ($I > 35/2$), it is the continuation of [541]1/2 sequence with no AB quasineutrons. An upper limit for the interaction strength between bands 5 and 6 can be determined as half the energy difference between the bands at the point where they lie closest to each other. From the inspection of Fig. 4(b), this occurs at $I = 35/2$, and the interaction strength is found to be $|V_{\max}| = 66$ keV. A similar band is found in ^{173}Ta [22], and the interaction strength was determined to be 88 keV through a two-band mixing calculation. Note also in Fig. 7(c) that an alignment gain occurs at approximately 0.37 MeV. This is likely the BC crossing in the continuation of the [541]1/2 structure. This crossing is also delayed with respect to the CSM predictions, presumably as a result of the larger deformation.

G. Band 7

Since band 7 strongly feeds the [541]1/2 band, it is tempting to assume that it is a vibrational band based on this structure. However, there is a difference of 4–5$\hbar$ in alignment between band 7 and the favored signature of the [541]1/2 band [Fig. 7(c)]. Therefore, this interpretation of band 7 is unlikely. Instead, a rotational band based on a three-quasiparticle excitation should be considered. As seen in Fig. 7(c), band 7 does not experience the AB alignment; thus, the A neutron is likely involved in the configuration. Since the $\nu i_{13/2}$ level is from a unique-parity orbital, the other neutron likely has negative parity. Band 7 is decoupled; therefore, this negative-parity neutron is perhaps from the [521]1/2 orbital as it exhibits significant signature splitting. Approximately 5$\hbar$ of alignment would result from these neutrons, and an additional 2–3$\hbar$ is required from the proton to match the observed alignment. As seen from Fig. 7, the most likely proton that will produce this value is one occupying the [541]1/2 orbital. Thus, a tentative configuration for band 7 is $\pi h_{9/2}\nu(i_{13/2}, p_{3/2})$, which would require the band to have positive parity in agreement with the proposed scheme of Fig. 1.

H. Band 8: The [514]9/2 structure

Li *et al.* [13] previously assigned band 8 as a sequence based on the [514]9/2 orbital. The initial alignment of $\sim$1.5$\hbar$ seen in Fig. 7(d) is consistent with this assignment, and the AB crossing is observed near 0.24 MeV. Calculated $B(M1)/B(E2)$ ratios for the [514]9/2 configuration are found to lie well above the experimental values [Fig. 8(b)] when using a quadrupole moment of $Q_0 = 5.5$ b. This is true both before and after the AB crossing as shown in the figure by lines 1 and 2, respectively. Calculated $B(M1)/B(E2)$ ratios were also found to be too large in the $\pi h_{11/2}$ band of ^{171}Re [35], where the authors determined that using a moment of $Q_0 = 6.5$ b reproduced the data more satisfactorily. Lines 3 and 4 in Fig. 8(b) represent theoretical calculations with this larger quadrupole moment, and an improved fit to the data is realized. Perhaps this indicates that this band in ^{169}Ta is more deformed than suggested in Ref. [14]. In fact, total Routhian surface calculations by Li *et al.* [13] predict a deformation of $\beta_2 = 0.245$ for the [514]9/2 band, which is significantly larger than the prediction of Ref. [14] where $\beta_2 = 0.216$ was calculated. The former value implies $Q_0 = 6.2$ b, which is in good agreement with the present data. There is a gradual gain in alignment above a frequency of 0.35 MeV, which is more apparent in the $\alpha = -1/2$ signature. The $\alpha = +1/2$ signature tracks the ground-state band of ^{168}Hf consistently to the highest observed frequency. The gradual gain in alignment is likely associated with the CD crossing where the interaction strength is larger in the $\pi h_{11/2}$ band than in the positive-parity bands. This is perhaps a further indication that the [514]9/2 band is more deformed than the positive-parity bands, as the interaction strength of this crossing is similar to that observed in the [541]1/2 band.

I. Bandhead energy systematics

In 1990, Nazarewicz, Riley, and Garrett produced a landmark paper [14] in which they systematically calculated deformations and bandhead energies for various proton orbitals in the rare-earth region by means of an approach utilizing a Woods-Saxon potential. Comparisons of these bandhead energies were carried out with the experimental data available at that time, and very good agreement was noted. However, no excitation energies for the lighter Ta ($A = 167$–171) nuclei were known. Now that bandhead energies have been experimentally established in these lighter nuclei, a new comparison with those predictions is warranted. The experimental energies for $^{167-183}$Ta are displayed in Fig. 13(a), while the calculated values from Ref. [14] are given in Fig. 13(b). Note that the energy of the $5/2^-$ state was used for the bandhead energy of the [541]1/2 orbital, as the $1/2^-$ state is often not observed. In addition, the energy of the $3/2^+$ state was used for the [411]1/2 bandhead energy in ^{171,173}Ta, because the $1/2^+$ state was not found in either nucleus. This has little impact since the $1/2^+$ level lies typically within 10–20 keV of the $3/2^+$ state.

In general, very good agreement between the experimental and theoretical values is found. The U-shape pattern of the [541]1/2 orbital can be understood, as this intruder orbital is closest to the Fermi surface when the ground-state deformation is largest (^{173}Ta) [14]. This trend is represented very well by the calculations, as seen in Fig 13(b). The largest discrepancy between theory and experiment occurs for the [411]1/2 band. In this case, the slope of excitation energy versus A is very well reproduced, but the predicted energies lie approximately 300–400 keV too high. Since the $d_{3/2}$[411]1/2 orbital lies below the Fermi surface for Ta, this suggests that the $d_{3/2}$ shell was calculated to lie too low in excitation energy. One may also note that the [514]9/2 orbital in the $A < 179$ nuclei is experimentally found to be at higher energies than calculated by theory. This discrepancy likely results from

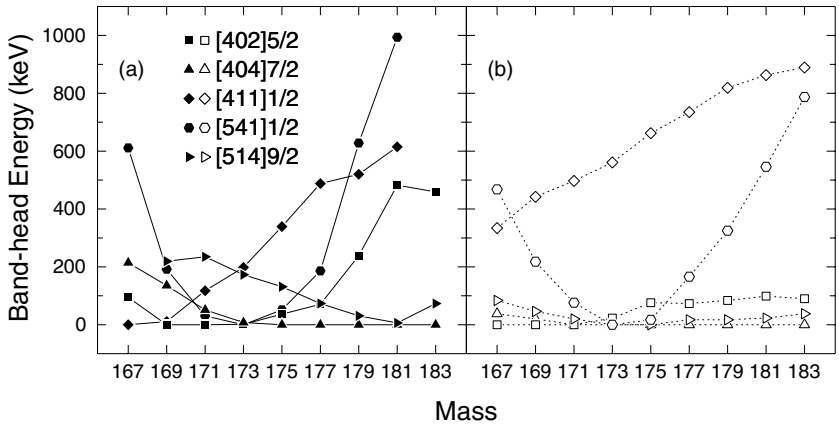

FIG. 13. Bandhead energies in the Ta isotopic chain. (a) Experimental. (b) Predicted from calculations based on Woods-Saxon potential of Ref. [14].

the possible larger deformation associated with the [514]9/2 band, as discussed above. Finally, it is interesting to note that the [402]5/2 orbital is experimentally found to increase in energy above where maximum deformation occurs ($A = 173$), while the [404]7/2 structure produces a near mirror image below $A = 173$ [see Fig. 13(a)]. Since deformation decreases on either side of $A = 173$, this indicates that the relative placements of the [402]5/2 and [404]7/2 proton orbitals are strongly dependent on neutron number.

V. SUMMARY

Although ^{169}Ta was produced in the relatively weak $6n$ channel of our fusion-evaporation reaction, the resolving power of Gammasphere made a significant extension of the level scheme possible. Four new bands were found, including the one associated with the [404]7/2 configuration. The latter mixes strongly with the [402]5/2 band as should be expected for pseudospin partners. The intruder [660]1/2 sequence was also identified for the first time in ^{169}Ta. This configuration has drawn considerable attention recently as wobbling bands have been observed in Lu nuclei based on this orbital. No wobbling structures were observed in ^{169}Ta. However, the possibility that a dedicated experiment with a more favorable reaction channel could reveal this exotic mode cannot be ruled out. The moment of inertia and the band crossing behavior of the $i_{13/2}$ sequence indicate that it likely has enhanced deformation with respect to the other configurations. However, a lifetime measurement is required to verify this assertion. The new data allowed the excitation energies of all the configurations to be determined for the first time. In general, good systematic agreement is observed between the Ta bandhead energies and the calculated values of Ref. [14].

ACKNOWLEDGMENTS

Special thanks to D. C. Radford and H. Q. Jin for their software support. The authors also thank the ANL operations staff at Gammasphere and gratefully acknowledge the efforts of J. P. Greene for target preparation and use. This work is funded by the National Science Foundation under Grant Nos. PHY-0300673 (USNA) and PHY-0139950 (FSU), as well as by the U.S. Department of Energy, Office of Nuclear Physics, under Contract Nos. W-31-109-ENG-38 (ANL) and DE-FG02-96ER40983 (UT).

[1] S. W. Ødegård *et al.*, Phys. Rev. Lett. **86**, 5866 (2001).
[2] D. R. Jensen *et al.*, Nucl. Phys. **A703**, 3 (2002).
[3] D. R. Jensen *et al.*, Phys. Rev. Lett. **89**, 142503 (2002).
[4] G. Schönwaßer *et al.*, Phys. Lett. **B552**, 9 (2003).
[5] H. Amro *et al.*, Phys. Lett. **B553**, 197 (2003).
[6] P. Bringel *et al.*, Eur. Phys. J. A **24**, 167 (2005).
[7] C. X. Yang *et al.*, Phys. Lett. **B133**, 39 (1983).
[8] J. C. Bacelar *et al.*, Nucl. Phys. **A442**, 547 (1985).
[9] D. J. Hartley *et al.*, Phys. Rev. C **72**, 064325 (2005).
[10] H. J. Jensen *et al.*, Nucl. Phys. **A695**, 3 (2001).
[11] S. Frauendorf, Phys. Scr. **24**, 349 (1981).
[12] W. Satula, R. Wyss, and F. Dönau, Nucl. Phys. **A565**, 573 (1993).
[13] S. G. Li *et al.*, Nucl. Phys. **A555**, 435 (1993).
[14] W. Nazarewicz, M. A. Riley, and J. D. Garrett, Nucl. Phys. **A512**, 61 (1990).
[15] R. V. F. Janssens and F. S. Stephens, Nucl. Phys. News **6**, 9 (1996).
[16] M. Cromaz *et al.*, Nucl. Instrum. Methods A **462**, 519 (2001).
[17] D. C. Radford, Nucl. Instrum. Methods A **361**, 297 (1995).
[18] F. Meissner, W.-D. Schmidt-Ott, V. Freystein, T. Hild, E. Runte, H. Salewski, and R. Michaelsen, Z. Phys. A **337**, 45 (1990).
[19] H. Song *et al.*, Chin. Phys. Lett. **20**, 346 (2003).
[20] Y. H. Zhang *et al.*, Eur. Phys. J. A **1**, 1 (1998).
[21] Y. H. Zhang *et al.*, Chin. Phys. Lett. **15**, 92 (1998).
[22] H. Carlsson *et al.*, Nucl. Phys. **A592**, 89 (1995).
[23] D. Barnéoud and C. Foin, Nucl. Phys. **A287**, 77 (1977).
[24] L. K. Peker, Nucl. Data Sheets **65**, 439 (1992).
[25] B. Singh and A. R. Farhan, Nucl. Data Sheets **89**, 1 (2000).
[26] E. M. Beck *et al.*, Z. Phys. A **327**, 397 (1987).
[27] F. Dönau, Nucl. Phys. **A471**, 469 (1987).
[28] A. Bohr and B. R. Mottelson, *Nuclear Structure* (Benjamin, New York, 1975), Vol. 2.
[29] R. D. Ratna Raju, J. P. Draayer, and K. T. Hecht, Nucl. Phys. **A202**, 433 (1973).
[30] R. Bengtsson, S. Frauendorf, and F.-R. May, At. Data Nucl. Data Tables **35**, 15 (1986).

[31] S. K. Tandel *et al*., Phys. Rev. C **73**, 044306 (2006).
[32] P. Möller and J. R. Nix, Nucl. Phys. **A536**, 20 (1992).
[33] D. R. Jensen *et al*., Eur. Phys. J. A **8**, 165 (2000).
[34] A. Aguilar *et al*. (in preparation).
[35] H. Carlsson *et al*., Nucl. Phys. **A551**, 295 (1993).
[36] A. Neußer-Neffgen *et al*., Phys. Rev. C **73**, 034309 (2006).
[37] J. D. Morrison, J. Simpson, M. A. Riley, H. W. Cranmer-Gordon, P. D. Forsyth, D. Howe, and J. F. Sharpey-Schafer, J. Phys. G **15**, 1871 (1989).